

# Simulation study on effects of loading rate on uniaxial compression failure of composite rock-coal layer

Shao J. Chen<sup>a</sup>, Da W. Yin<sup>\*</sup>, N. Jiang<sup>\*\*</sup>, F. Wang<sup>b</sup> and Wei J. Guo<sup>c</sup>

College of Mining and Safety Engineering, Shandong University of Science and Technology, 579 Qianwanggang Road, Huangdao District, Qingdao, Shandong Province, 266590, China

(Received October 6, 2018, Revised February 19, 2019, Accepted February 21, 2019)

**Abstract.** Geological dynamic hazards during coal mining can be caused by the failure of a composite system consisting of roof rock and coal layers, subject to different loading rates due to different advancing velocities in the working face. In this paper, the uniaxial compression test simulations on the composite rock-coal layers were performed using PFC<sup>2D</sup> software and especially the effects of loading rate on the stress-strain behavior, strength characteristics and crack nucleation, propagation and coalescence in a composite layer were analyzed. In addition, considering the composite layer, the mechanisms for the advanced bore decompression in coal to prevent the geological dynamic hazards at a rapid advancing velocity of working face were explored. The uniaxial compressive strength and peak strain are found to increase with the increase of loading rate. After post-peak point, the stress-strain curve shows a steep stepped drop at a low loading rate, while the stress-strain curve exhibits a slowly progressive decrease at a high loading rate. The cracking mainly occurs within coal, and no apparent cracking is observed for rock. While at a high loading rate, the rock near the bedding plane is damaged by rapid crack propagation in coal. The cracking pattern is not a single shear zone, but exhibits as two simultaneously propagating shear zones in a “X” shape. Following this, the coal breaks into many pieces and the fragment size and number increase with loading rate. Whereas a low loading rate promotes the development of tensile crack, the failure pattern shows a V-shaped hybrid shear and tensile failure. The shear failure becomes dominant with an increasing loading rate. Meanwhile, with the increase of loading rate, the width of the main shear failure zone increases. Moreover, the advanced bore decompression changes the physical property and energy accumulation conditions of the composite layer, which increases the strain energy dissipation, and the occurrence possibility of geological dynamic hazards is reduced at a rapid advancing velocity of working face.

**Keywords:** composite rock-coal layer; loading rate; stress-strain behavior; strength and failure characteristics; advanced bore decompression

## 1. Introduction

During deep coal mining process, geological dynamic hazards frequently occur in many coal mines of China, such as rock burst, coal and gas outburst, causing potential safety hazards for coal production safety (Pan *et al.* 2003, Liu *et al.* 2018, Wang *et al.* 2017, Hua *et al.* 2018). A number of research outcomes and engineering practices have demonstrated that geological dynamic hazards in coal mining are caused by the catastrophic instability and failure of a combined system consisting of roof rock and coal layers (Lu *et al.* 2015, Zhao *et al.* 2016, Chen *et al.* 2016,

Chen *et al.* 2018, Wang *et al.* 2019). In mining engineering, the roof rock and coal layers in front of the working face are loaded at different loading rates due to the varied advancing velocities (Zhang *et al.* 2017, Xie *et al.* 2007, Yang *et al.* 2016). There are great differences in the mechanical properties of composite rock-coal layers at different loading rates. Therefore, it is of great significance to study the deformation and failure behaviors of composite rock-coal layers at different loading rates for preventing geological dynamic hazards and ensuring the safety production in mining engineering.

Many studies have focused on the deformation and failure behaviors of the composite rock-coal layer through theoretical analysis, physical tests and numerical simulations. Based on the Coulomb-Mohr yielding criteria, a failure criterion for the composite rock-coal layer was established and discussed (Landriani and Taliercio 1987). Petukhov and Linkov (1979) analyzed the stability of the general bipartite and rock-coal systems while studying the stable behavior of rock mass after post-peak point. Four types of three-layer composed models of rock and coal with different strengths and stiffness were established and their failure characteristics were studied (Zhao *et al.* 2014). The strength characteristics and failure behavior of a composite sandstone-coal layer with identical heights under triaxial

\*Corresponding author, Ph.D.

E-mail: 949251142@qq.com

\*\*Corresponding author, Ph.D.

E-mail: 150653034@qq.com

<sup>a</sup>Associate Professor

E-mail: csjwyb@163.com

<sup>b</sup>Ph.D.

E-mail: 412863764@qq.com

<sup>c</sup>Associate Professor

E-mail: Wjguo@sdu.edu.cn

compression were analyzed (Zuo *et al.* 2011). The effects of height ratio of rock to coal on the strength, macroscopic failure initiation and failure characteristics of the composite sandstone-coal layer were studied (Chen *et al.* 2017). Meanwhile, the effects of loading and unloading rate on the deformation and failure behavior of the composite rock-coal layer were analyzed (Huang and Liu 2013). The effects of rock strength on the failure mode and mechanical behavior of the composite rock-coal layer were discussed (Liu *et al.* 2015). Through experimental and numerical investigations, the influences of the interface angel on the strength and failure characteristics of a composite rock-coal layer were analyzed (Zhao *et al.* 2016, Guo *et al.* 2011). Using the RFPA<sup>2D</sup> software, Guo *et al.* (2018) studied the mechanical behaviors of composite rock-coal-rock layers with different coal thicknesses. Yin *et al.* (2018a, b) analyzed the effects of joint length and joint angle in coal on the mechanical behavior of composite rock-coal layer.

The aforementioned achievements are important to understand the deformation and failure behaviors of the composite rock-coal layer. However, few studies have been conducted on the effects of loading rate on the composite layer. Meanwhile, the researches of loading rates effects on the deformation and failure characteristics are more focused on the single rock or coal specimens (Lajtai *et al.* 1991, Chong *et al.* 1980, Yin *et al.* 2010, Blanton 1981). Additionally, because the capability of nondestructive testing and monitoring methods is still limited, it is difficult to observe the process of mechanical response of the material, limiting people's understanding of the mechanical response mechanism of rock and coal material through physical tests. Moreover, due to the discreteness of physical properties of the rock and coal specimens in physical tests, the test results are difficult to grasp the whole picture of the research object (Zhang *et al.* 2016). The particle flow code (PFC) is an effective method to study the macro-mechanics problems at the micro-level. It can essentially reveal the deformations and failure mechanisms of coal or rock, which has been widely applied in uniaxial compression test simulations and triaxial compression test simulations (Lavrov 2001, Lee and Jeon 2011, Kulatilake *et al.* 2001, Park and Song 2009).

In this paper, the uniaxial compression test simulations on the composite rock-coal layers at the different loading rates were conducted using PFC<sup>2D</sup> software and the purpose was to interpret the effecting mechanism of loading rate on stress-strain behavior, strength and characteristics and crack nucleation, propagation and coalescence in the composite rock-coal layer. Considering the composite layer, the mechanisms of the advanced bore decompression in coal to prevent geological dynamic hazards at a rapid advancing velocity in working face were simulated and discussed.

## 2. Problem formulation

The exploitation of coal resources breaks the equilibrium state of local stress fields in the mining area. The development and evolution of stress field are dynamic and vary in time and space. A lot of theoretical and experimental studies have shown that after the working face

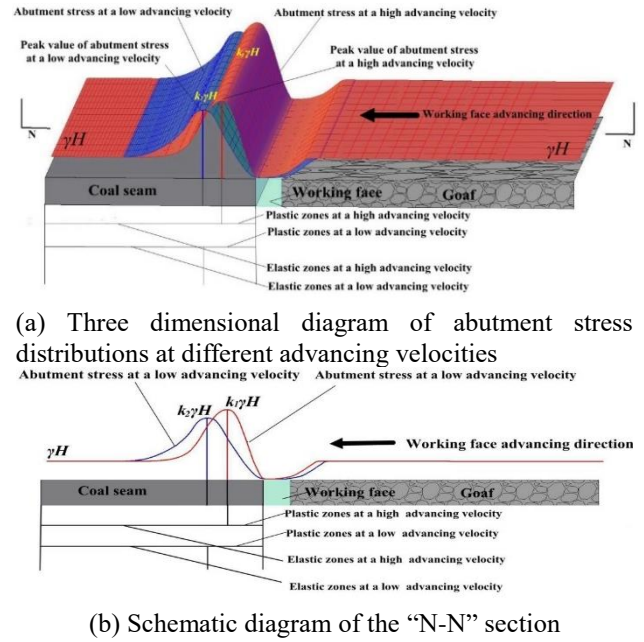


Fig. 1 Abutment stress distribution of surrounding rocks at different advancing velocity

is mined, a stress concentration will occur in coal seam in the front of working face and the abutment stress increases firstly and then decreases. Additionally, the peak value of abutment stress is located at the junction of the plastic zone and elastic zone in coal seam. When the advancing velocity is high, the stress concentration degree and peak value of abutment stress will increase, showing a large possibility of geological dynamic hazards in the working face (Zhang *et al.* 2017, Xie *et al.* 2007, Xing *et al.* 2017). The stress concentration degree and peak value of abutment stress at a low advancing velocity will slightly decrease instead. Moreover, the peak point at a high advancing velocity will be much closer to the coal wall than that at a low advancing velocity. Consequently, the plastic zone size decreases at a high advancing velocity and increases at a low advancing velocity, as shown in Fig. 1.  $k_1$  and  $k_2$  are the stress concentration factors at high and low advancing velocities, respectively ( $k_1 > k_2$ ).  $\gamma$  is the average bulk density of overlying strata.  $H$  is the mining depth. Under the given working face length and width, the abutment stress in coal seam in the front of the working face can be confirmed by the follow Eq. (1) (Zhang *et al.* 2017, Xie *et al.* 2007)

$$\sigma = \left[ \left( \frac{ax^b}{\varepsilon_0 h} \right)^m + 1 \right] \exp \left[ - \left( \frac{ax^b}{\varepsilon_0 h} \right)^m \right] \times \left[ \frac{E_0 ax^b}{h} + \frac{\eta abx^{b-1}}{h} \left( 1 - e^{-\frac{E_0 t}{\eta}} \right) \right] \quad (1)$$

where  $\sigma$  is the abutment stress in coal seam in the front of the working face;  $x$  is the distance from peak point to coal wall, denoting the plastic zone size;  $h$  is the coal seam thickness;  $t$  is the mining time;  $a$ ,  $b$ ,  $\varepsilon_0$ ,  $m$ ,  $\eta$  and  $E_0$  are constants determined by the laboratory tests.

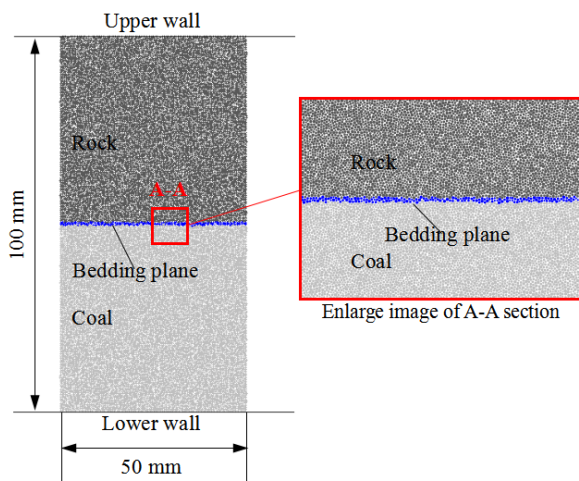
## 3. Numerical model

### 3.1 Micro-parameters of roof rock and coal

In PFC<sup>2D</sup> software, the parallel bond model refers to

Table 1 Micro-parameters of rock and coal (Zhao *et al.* 2016, Guo *et al.* 2018, Yin *et al.* 2018a, b)

Parameters	Rock	Coal	Parameters	Rock	Coal
Minimum particle size/mm	0.2		Parallel particle contact elastic modulus/GPa	12	4
Particle size ratio	1.5		Parallel bond normal strength/MPa	45	15
Density/ ( kg/m <sup>3</sup> )	2600	1800	Parallel bond tangential strength/MPa	45	15
Contact modulus of the particle/GPa	12	4	Parallel normal stiffness/tangential stiffness	2.5	
Parallel bond radius multiplier	1		Normal stiffness/tangential stiffness	2.5	
Coefficient of friction			0.5		

Fig. 2 PFC<sup>2D</sup> model for composite rock-coal layer

plane-to-plane bond and the moment of force can be well transmitted (Zhao *et al.* 2015). Therefore, it is applied to simulating the compact material, such as rock and coal. In this investigation, the uniaxial compression model for the composite rock-coal layer was built using the parallel bond model.

In the parallel bond model, the macroscopic mechanical properties of the roof rock and coal are mainly affected by the micro-parameters of particles in PFC<sup>2D</sup> software (Yin *et al.* 2018a), i.e., contact modulus of the particle, parallel grain contact elastic modulus, parallel bond normal strength, parallel bond tangential strength, etc. The determinations of these micro-parameters are the processes of minimizing the error between simulation and experimental results, and they are obtained by adjusting the micro-parameters to match the elastic moduli, Poisson's ratios, peak stresses of standard roof rock and coal specimens ( $\Phi$  50 mm $\times$ 100 mm) achieved by the laboratory tests. Due to the limitation of laboratory test condition, the micro-parameters of rock and coal provided by Zhao *et al.* (2016), Guo *et al.* (2018) and Yin *et al.* (2018a, b) were used to carry out the numerical tests, as shown in Table 1.

### 3.2 PFC<sup>2D</sup> model construction

In this study, the rock and coal are freely superimposed into a composite layer and the contact surface is the bedding

plane without a cohesive force. A particle flow model for composite rock-coal layer is established and generated by radius extension, as shown in Fig. 2. The length and height of the model are 50 mm and 100 mm, respectively. The heights of rock and coal in the composite layer are both 50 mm. In this model, the minimum particle radius is 0.2 mm, and the maximum radius is 0.3 mm. There are 21390 particles generated in the model. The bedding plane is generated by the JSET command. For facilitating the distinction, the particles through the bedding are colored in blue. Based on various researches, the micro-parameters of the bedding plane are weakened and set as very small values (Kulatilake *et al.* 2001, Zhao *et al.* 2016, Park and Song 2001, Guo *et al.* 2018). The friction coefficient was set as 0.1, and the parallel bond compressive strength and parallel bond cohesive strength were all set as zero.

### 3.3 Numerical test conditions

Now, the uniaxial compression model for the composite rock-coal layer is well built. The unbalanced force generated in this process is eliminated cyclically. The wall is lengthened appropriately for preventing the spill-out of particles. Loading is performed by moving the upper and lower walls.

In order to thoroughly study the effects of loading rate on the mechanical behavior of composite rock-coal layer, the loading rates at different loading intervals are selected as 0.001 m/s, 0.005 m/s, 0.050 m/s and 0.500 m/s (Zhang *et al.* 2016; Yin *et al.* 2010). Loading is terminated when the axial stress is 10% of the peak stress.

## 4. Numerically simulated results

### 4.1 Effects of loading rate on the stress-strain behavior

The complete stress-strain curves of the composite rock-coal layers and single granite layers (Zhang *et al.* 2016) under uniaxial compression with different loading rates are presented in Fig. 3.

In Fig. 3, it can be seen that the complete stress-strain curves of composite rock-coal layers under uniaxial compression are quite similar at different loading rates, basically consistent with that of single granite layers. The stress-strain curve generally can be divided into four stages, ranging from linear elastic deformation stage, non-linear deformation stage, post-peak strain softening to the residual strength stage. The loading rate affects the axial strain values required for each stage. At the initial stage, i.e., the initial stage of linear elastic deformation stage, due to the lack of sufficient time, the composite layer has little time to occur adaptive deformation for adapting a high loading rate, and the uneven distribution of unbalance force occurs in the process of stress loading. The stress-strain curve shows a steep rise, which also can be found in the single granite layer at the loading rate of 0.500 m/s. However, at a low loading rate, there is enough time for composite layer to adapt the loading rate, the stress-strain curve presents a straight rise. In the post-peak region, the initial damage and

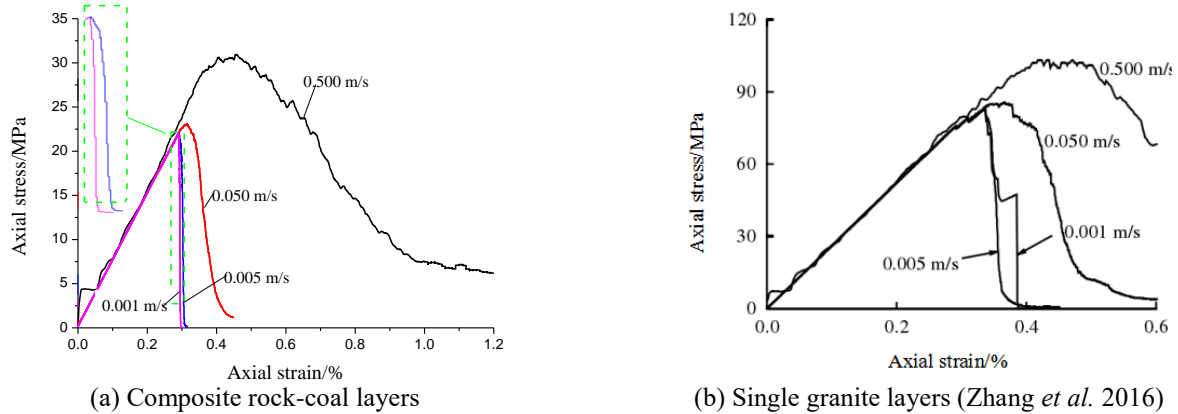


Fig. 3 Stress-strain curves of composite rock-coal layers and single granite layers under different loading rates

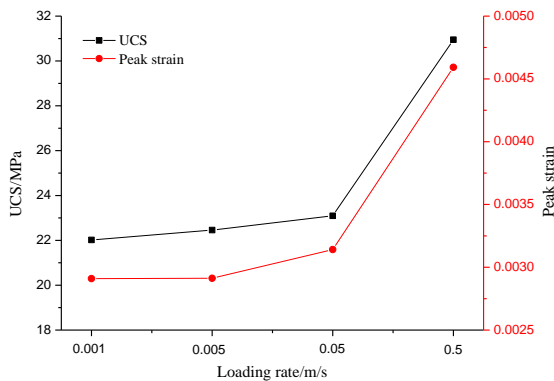


Fig. 4 Relationships between UCS, peak strain and loading rate

Table 2 Numerical test results of uniaxial compression on composite rock-coal layers under different loading rates

0.001	22.02	0.00281
0.005	22.46	0.00291
0.050	23.095	0.00314
0.500	30.948	0.00459

newborn crack have sufficient time to propagate and develop further at a low loading rate, resulting in a steep stepped drop in the stress-strain curve. However, the post-peak stress-strain curve at a high loading rate presents a smoothing progressive decrease instead, which is also shown in single granite layers. These achievements are similar to the effects of loading rate on the stress-strain behavior of single granite layers, as shown in Fig. 3 (b). In addition, the elastic modulus almost does not change with the loading rate, this is principally because that there is no initial compression stage in PFC<sup>2D</sup> software, which is different from the physical test. This phenomenon has been also found in previous simulation studies using PFC<sup>2D</sup> software (Kulatilake *et al.* 2001, Zhao *et al.* 2016, Yin *et al.* 2018a, b).

#### 4.2 Effects of loading rate on the strength and deformation properties

The numerical test results are presented in Table 2. The relationships between uniaxial compressive strength (UCS),

peak strain and loading rate are given in Fig. 4.

In Table 2 and Fig. 4, with the increase of the loading rate, UCS and its corresponding strain increase nonlinearly. The high loading rate enhances the strength of the composite rock-coal layer. This is because at a high loading rate, the composite layer will generate more microcracks as shown in Fig. 5 and thus more energies are required. Meanwhile, there is not enough time for energy accumulation with a short loading time. Therefore, according to the energy theorem or function theorem, the composite layer can only offset the external energy by increasing its strength. The composite layer strength increases with the loading rate. Additionally, due to the failure of composite layer mainly occurs within coal, as shown in Fig. 5, the structural strength of composite layer is seriously determined by the coal strength. The enhancing effect of a high loading rate on strength is mainly for coal, and the structural strength of composite layer increases.

Compared to UCS at the loading rate of 0.001 m/s, UCS at the loading rates of 0.005 m/s, 0.050 m/s and 0.5 m/s, increase by 1.998%, 4.882% and 40.545%, respectively, and the corresponding peak strains increase by 3.928%, 12.143% and 63.929%, respectively.

#### 4.3 Effects of loading rate on macro-failure modes

The propagation and coalescence of microcracks form the main control failure crack, causing the final failure of the composite rock-coal layer. Fig. 5 shows the macro-failure modes of composite layers under different loading rates. In Fig. 5, a microcrack is represented as a black segment, and a macroscopic shear failure crack and a macroscopic tensile crack represented as a thick red line and a thick yellow line, respectively.

In Fig. 5, the failures of composite rock-coal layers under different loading rates mainly occur within coal, and no apparent failure is observed for rock. However, when the loading rate is high of 0.500 m/s, the rock near the bedding plane is destroyed by the crack propagation in coal, as shown in a blue line box of Fig. 5(d). This is because that the strength of rock near the bedding plane is weakened by the frictional restraint stress caused by the differences in elastic moduli and Poisson's ratios of rock and coal. The high loading rate can significantly increase the crack propagation in coal, causing the failure of rock near the

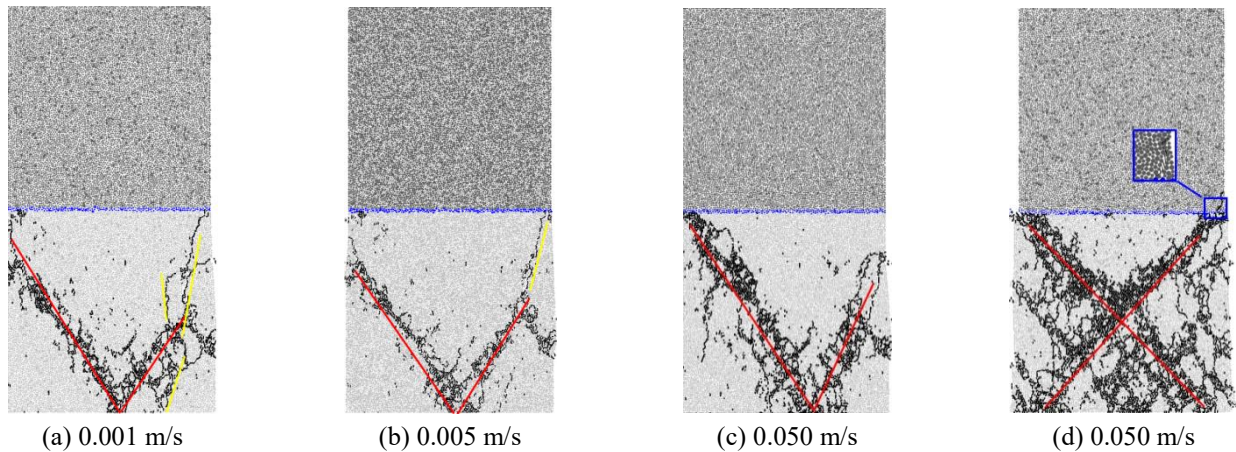


Fig. 5 Failure modes of composite rock-coal layers under different loading rates

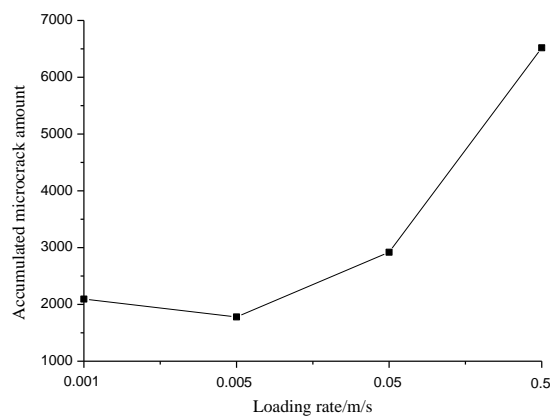


Fig. 6 Accumulated microcrack amounts of composite rock-coal layers under different loading rates

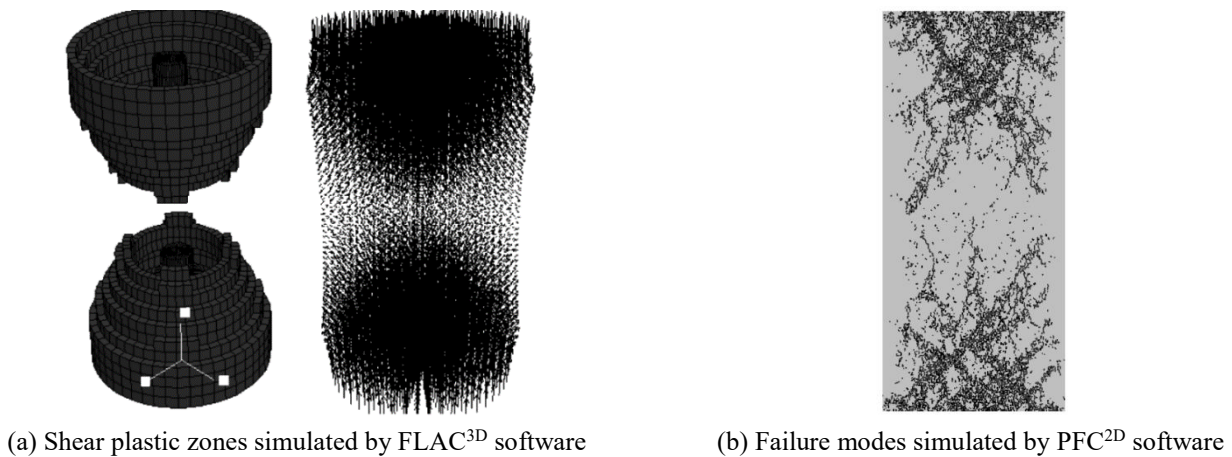


Fig. 7 Failure modes of single rock samples at a high loading rate (Yin *et al.* 2010)

bedding plane.

Additionally, the failure models of composite rock-coal layers under different loading rates are not quite similar to each other. With the increase of loading rate, the failure models change from local failure instability of coal to its overall failure instability. The composite layer at the loading rate of 0.500 m/s becomes more broken and there are 6519 microcracks, as shown in Fig. 6, implying a higher possibility of geological dynamic hazards occurrence of the composite layer at a high loading rate. The main control

failure crack is a X-shaped shear failure, showing that the development advantages of dominant shear zones at a high loading rate are limited and the shear zones achieve a simultaneous development, thus form the X-shaped shear failure. This phenomenon is also found in single rock or specimen at a high loading rates, as shown in Fig. 7 (In Fig 7(b), a microcrack is represented as a black segment and the specimen size is 50 mm×150 mm). Whereas when the loading rates are 0.001 m/s, 0.005 m/s, 0.050 m/s, the failure models are mainly the shear failure, but

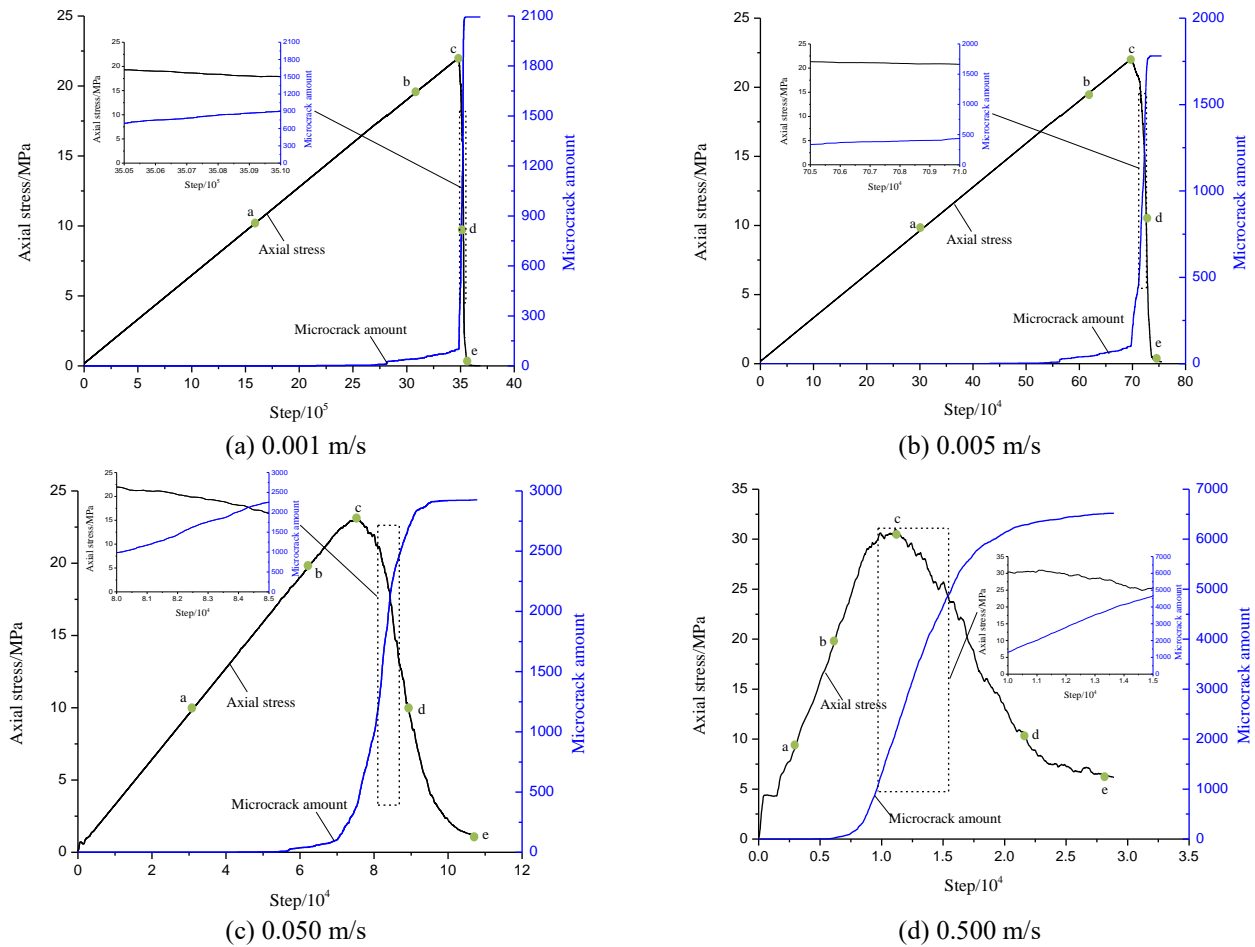


Fig. 8 Relationships between the microcrack amount evolutions and axial stresses under different loading rates

accompanied with tensile failure at loading rates of 0.001 m/s and 0.005 m/s. Therefore, the failure model at the loading rate of 0.050 m/s is an V-shaped shear failure. The failure models at the loading rates of 0.001 m/s and 0.005 m/s are V-shaped hybrid failure of shear failure and tensile failure. Meanwhile, the width of main control shear failure zones increases with the loading rate, which can be verified by the failure models in Fig. 5 and accumulated microcrack amounts represented in Fig. 6. In Fig. 6, when the loading rate increases from 0.001 m/s to 0.500 m/s, the accumulated microcrack amount increases from 2094 to 6519. However, the accumulated microcrack amount at the loading rate of 0.001 m/s is slightly larger than that at the loading rate of 0.005 m/s. This is because that the tensile cracks at a low loading rate can adequately propagate and develop.

## 5. Crack propagation and coalescence under different loading rates

### 5.1 Microcrack amount evolution

Fig. 8 illustrates the relationships between the microcrack amount evolutions and axial stresses of composite rock-coal layers under different loading rates.

The microcrack amount generally increases with the deformation, and the increasing rate of microcrack amount

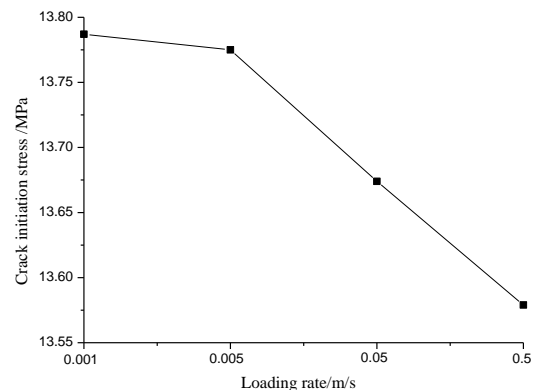


Fig. 9 Relationship between a crack initiation stress and loading rate

evolves during the process of crack initiation, propagation and coalescence. The evolution characteristics of the microcrack amount in linear elastic deformation stage, non-linear deformation stage, post-peak strain softening stage and the residual strength stage of composite rock-coal layer are basically similar under different loading rates. In the linear elastic deformation stage, only when the axial stress reaches up to crack initiation stress, a few microcracks can be observed in the accumulated microcrack number curve. Fig. 9 shows the crack initiation stresses under different loading rates. In Fig. 9, with the increase of loading rate, the

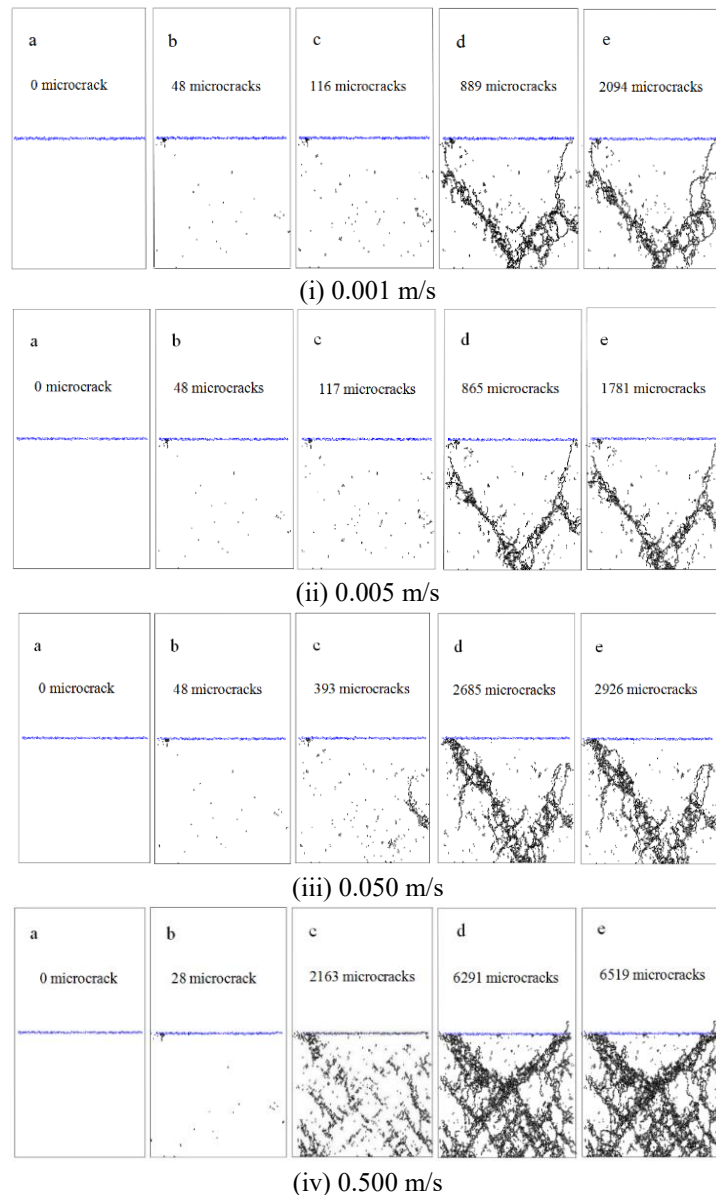


Fig. 10 Progressive failure processes of composite rock-coal layers under different loading rates

crack initiation stress generally decreases with a slight decrease. From the stage of linear elastic deformation to nonlinear deformation, more microcracks are generated, verified from a slow increase in the accumulated microcrack amount curve. And now the composite layer is in the stable micro-fracture propagation stage. After peak stress, the microcrack amount increases faster than other phases. The accumulated microcrack amount curve presents a steep rise. In order to compare the microcrack growth rate in post-peak strain softening stage, the accumulated microcrack amount curve during 5000 steps in the post-peak strain softening stage are separately drawn, as shown in the black dashed box of Fig. 8. The microcrack growth rate at a high loading rate is larger than that at a low loading rate, implying more broken of the composite layer under a high loading rate. Additionally, in the stage of the residual strength, a few microcracks are still generated, but the increase rate in this stage is much smaller than that of former stage.

### 5.2 Crack propagation and coalescence

In order to analyze the crack propagation and coalescence of the composite rock-coal layers under different loading rates, Fig. 10 gives the microcrack distributions in “a” point, “b” point, “c” point and “d” point of the stress-step curves in Fig. 8. Among them, “a” point corresponds to the axial stress of 10 MPa, “b” point corresponds to the axial stress of 20 MPa, “c” point corresponds to the peak stress, “d” point corresponds to the axial stress of 10MPa after peak and “e” point corresponds to the residual strength.

In the linear elastic deformation stage, under axial loading, the stress intensity transmitted between particles is less than the bonding strength between particles, thus no microcrack is generated in this stage, as shown in Fig. 10 (a). With the further increase of axial stress, when the stress intensity transmitted between particles is larger than the bonding strength between particles, microcracks are

generated. In Fig. 10 (b), microcracks are randomly distributed in coal. When the axial stress is 20 MPa, the microcrack amount at the loading rates of 0.001 m/s, 0.005 m/s and 0.05 m/s are basic equality. However, at this time, microcrack amount at the loading rate of 0.5 m/s is smaller than that at other loading rate. Due to the rapid loading rate, this phase is a transitional period from no microcracks to rapid growth of microcracks and this process is very short. At the peak stress, the microcrack amount at a high loading rate is much larger than that at a low loading rate. In Fig. 10, the microcracks aggregate into nucleation for forming crack source at the loading rates of 0.500 m/s and 0.05 m/s. After peak stress, the previously formed microcracks propagate and coalesce at a high rate to form the main control failure crack of composite layer. The crack propagation and coalescence rate at a high loading rate is much greater than that at a low loading rate. Thus the composite layer is severely destroyed. At the residual strength stage, the composite layer loses stability and its failure is mainly due to the friction sliding along the macroscopic crack.

## 6. Mechanism of advanced bore decompression in coal at a rapid advancing velocity

According to the above analysis, a high loading rate make the composite rock-coal layer more broken with a fast crack propagation and coalescence rate. Thus in mining engineering, a rapid advancing velocity can greatly enhance the occurrence possibility of geological dynamic hazards in the working face. While a rapid advancing velocity can improve coal production and bring more economic benefits. Therefore, how to coordinate the relationship of rapid advancing velocity and preventing geological dynamic hazards becomes a urgent problem to be solved. On the one hand, appropriately reduce the advancing velocity for preventing geological dynamic hazards. On the other hand, the advanced bore decompression for preventing geological dynamic hazards was proposed under the premise of keeping a rapid advancing velocity, widely used in many coal mines (Xie *et al.* 2007; Yang *et al.* 2016). Its basic principle is that the coal in the front of the working face is drilled to relieve pressure for preventing geological dynamic hazards. Through uniaxial compression tests of the cement specimens with pressure-relief boreholes for simulating coal specimens, the mechanisms of advanced bore decompression for preventing geological dynamic hazards were studied and analyzed (Liu *et al.* 2014). But the effects of advanced bore decompression on the composite rock-coal layer are neglected. Thus taking the composite layer as the research subject, the uniaxial compression test on composite layer with a pressure-relief borehole was simulated at a high loading rate of 0.500 m/s. The mechanisms of advanced bore decompression at a rapid advancing velocity were studied and analyzed.

The numerical model for advanced bore decompression uses the numerical model for a composite rock-coal layer under different loading rates. A pressure-relief borehole with a diameter of 10 mm is located in the central position of coal, as shown in Fig. 11. The numerical test results are

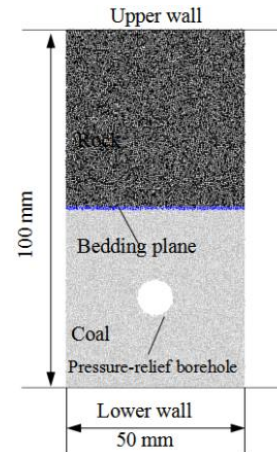


Fig. 11 Numerical model for composite rock-coal layer with a pressure-relief borehole

Table 3 Numerical results of uniaxial compression tests on composite rock-coal layers without and with a pressure-relief borehole

Test conditions	loading rate/m/s	UCS /MPa	Peak strain	Elastic modulus /GPa	Maximum strain energy/N-m
A composite layer without pressure-relief boreholes		30.948	0.00459	8.575	149.55
A composite layer with a pressure-relief borehole	0.500	24.146	0.00329	7.235	94.179

presented in Table 3. Complete stress-strain curves and strain energy variation laws of the composite rock-coal layers without and with a pressure-relief borehole under uniaxial compression are presented in Fig. 12.

From Table 3 and Fig. 12, the mechanisms of advanced bore decompression for preventing the geological dynamic hazards are mainly in two aspects. One is that changing the physical property and energy accumulation conditions of the composite layer. The other is that increasing the dissipation of strain energy of the composite layer. Compared the intact composite layer, UCS and peak strain of the composite layer with a pressure-relief borehole decrease by 21.98% and 28.32%, respectively. Meanwhile, changing the energy accumulation conditions is mainly to reduce the elastic modulus. Compared the intact composite layer, the elastic modulus decreases by 15.63%. It is well known that the occurrence of geological dynamic hazards is caused by the sudden release of accumulated strain energy. While the accumulation of strain energy has an important relationship with the elastic modulus. Therefore, the advanced bore decompression reduces the elastic modulus and then the strain energy accumulation decreases. Finally the occurrence possibility of geological dynamic hazards was reduced. Meanwhile, compared the intact composite layer, the maximum strain energy decreases by 37.03%, indicating the dissipation of strain energy. Moreover, after peak stress, elastic energy release of the composite layer with a pressure-relief borehole, is much slower than that of the intact composite layer, indicating a low occurrence

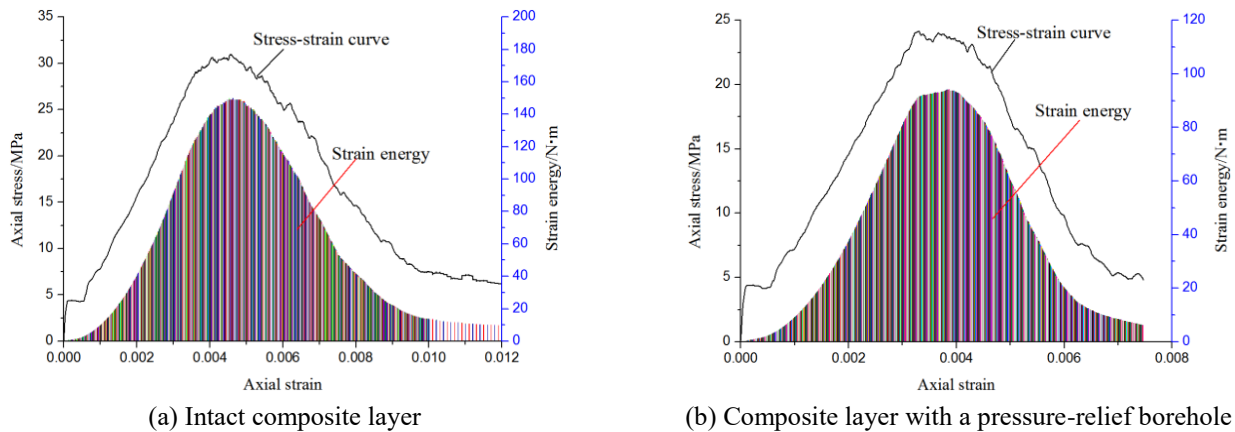


Fig. 12 Stress-strain curves and strain energy variation laws of composite rock-coal layers without and with a pressure-relief borehole

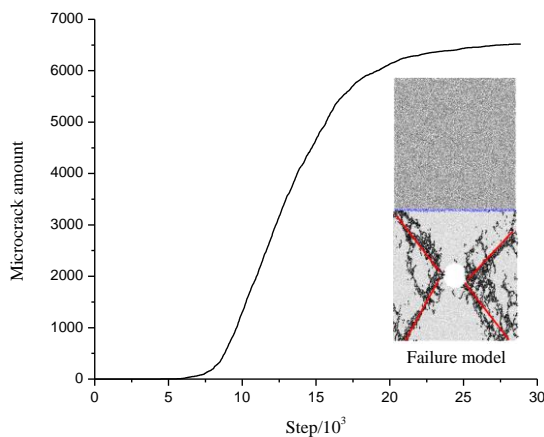


Fig. 13 Failure mode and microcrack amount evolution of the composite rock-coal layer with a pressure-relief borehole

possibility of geological dynamic hazards.

Finally, Fig. 13 shows the failure mode of the composite layer with a pressure-relief borehole. In Fig. 13, the fragmentation degree of the composite layer is reduced with 3713 microcracks. Its failure model is an X-shaped shear failure around the pressure-relief borehole. Also, the width of the main control shear failure zone decreases.

## 7. Conclusions

Based on the above numerical results, the following conclusions can be drawn:

- With an increase of the loading rate, the uniaxial compressive strength and peak strain of the composite rock-coal layer increases nonlinearly. After post-peak point, the stress-strain curve of the composite layer shows a steep drop at a low loading rate, while the stress-strain curve demonstrates a smoothing progress decrease at a high loading rate.

- The cracking of the composite rock-coal layer mainly occurs within coal, and no apparent cracking is observed for rock. Under a high loading rate, the roof rock near the bedding plane will be cracked by the rapid crack propagation in coal.

- The cracking pattern varies with an increase of the loading rate. The larger the loading rate is, the dominant the shear zone is. The failure mode at a high loading rate shows a X-shaped shear failure pattern. The coal fragment size becomes larger due to the rapid propagation and coalescence of microcracks. At a low loading rate, the tensile cracks propagation produces a V-shaped hybrid tensile and shear failure path. The width of the main shear failure zones increases with the loading rate.

- The mechanisms of advanced bore decompression for preventing the geological dynamic hazards at a rapid advancing velocity in the working face, mainly act in two aspects: One is that changing the physical property and energy accumulation conditions of the composite rock-coal layer. The other is that increasing the dissipation of strain energy of the composite layer.

## Acknowledgements

This study was supported by the National Natural Science Foundation of China (51474134, 51774194, 51874189, 51804179), Shandong Provincial Natural Science Foundation for Distinguished Young Scholars (JQ201612), Major basic research projects of Shandong Natural Science Foundation (ZR2018ZC0740), Taishan Scholars Project, Taishan Scholar Talent Team Support Plan for Advantaged & Unique Discipline Areas, Shandong Provincial Key Research and Development Plane (2017GSF17112), Key Research and Development Plane of China (2018YFC0604704).

## References

- Blanton, T.L. (1981), "Effect of strain rate from  $10^{-2}$  to  $10 \text{ sec}^{-1}$  in triaxial compression tests on three rocks", *Int. J. Rock Mech. Min. Sci.*, **18**(1), 47-62.
- Chen, S.J., Qu, X., Yin, D.W., Liu, X.Q., Ma, H.F. and Wang, H.W. (2018), "Investigation lateral deformation and failure characteristics of strip coal pillar in deep mining", *Geomech. Eng.*, **14**(5), 421-428.
- Chen, S.J., Yin, D.W., Cao, F.W., Liu, Y. and Ren, K.Q. (2016), "An overview of integrated surface subsidence-reducing

- technology in mining areas of China”, *Nat. Hazards*, **81**(2), 1129-1145.
- Chen, S.J., Yin, D.W., Zhang, B.L., Ma, H.F., and Liu, X.Q. (2017), “Study on mechanical characteristics and progressive failure mechanism of roof-coal pillar structure body”, *Chin. J. Rock Mech. Eng.*, **37**(7), 1588-1598 (in Chinese).
- Chong, K.P., Hoyt, P.M., Smith, J.W., and Paulsen, B.Y. (1980), “Effects of strain rate on oil shale fracturing”, *Int. J. Rock Mech. Min. Sci.*, **37**(1), 35-43.
- Guo, D.M., Zuo, J.P., Zhang, Y. and Yang, R.S. (2011), “Research on strength and failure mechanism of deep coal-rock combination bodies of different inclined angles”, *Rock Soil Mech.*, **32**(5), 1333-1339 (in Chinese).
- Guo, W.Y., Tan, Y.L., Yu, F.H., Zhao, T.B., Hu, S.C., Huang, D.M. and Qin, Z. (2018), “Mechanical behavior of rock-coal-rock specimens with different coal thicknesses”, *Geomech. Eng.*, **15**(4), 1017-1027.
- Hua, Y., Nie, W., Cai, P., Liu, Y.H., Peng, H.T. and Liu, Q. (2018), “Pattern characterization concerning spatial and temporal evolution of dust pollution associated with two typical ventilation methods at fully mechanized excavation faces in rock tunnels”, *Powder Technol.*, **334**, 117-131.
- Huang, B.X. and Liu, J.W. (2013), “The effect of loading rate on the behavior of samples composed of coal and rock”, *Int. J. Rock Mech. Min. Sci.*, **61**, 23-30.
- Kulatilake, P.H.S.W., Malama, B. and Wang, J. (2001), “Physical and particle flow modeling of jointed rock block behavior under uniaxial loading”, *Int. J. Rock Mech. Min. Sci.*, **38**(5), 641-657.
- Lajtai, E.Z., Duncan, E.J.S. and Carter, B.J. (1991), “The effect of strain rate on rock strength”, *Rock Mech. Rock Eng.*, **24**(2), 99-109.
- Landriani, G.S. and Taliercio, A. (1987), “A note on failure conditions for layered materials”, *Meccanica*, **22**(2), 97-102.
- Lavrov, A. (2001), “Kaiser effect observation in brittle rock cyclically loaded with different loading rates”, *Mech. Mater.*, **33**(11), 669-677.
- Lee, H. and Jeon, S. (2011), “An experimental and numerical study of fracture coalescence in pre-cracked specimens under uniaxial compression”, *Int. J. Solids Struct.*, **48**(6), 979-999.
- Liu, J., Wang, E.Y., Song, D.Z., Wang, S.H. and Niu, Y. (2015), “Effect of rock strength on failure mode and mechanical behavior of composite samples”, *Arab. J. Geosci.*, **8**(7), 4527-4539.
- Liu, J.H., Jiang, F.X., Sun, G.J., Zhang, Z.G. and Tan, W.F. (2014), “Mechanism of intensive venting pulverized coal to prevent coal burst and its application”, *Chin. J. Rock Mech. Eng.*, **33**(4), 747-754 (in Chinese).
- Liu, Q., Nie, W., Hua, Y., Peng, H.T. and Liu, Z.Q. (2018), “The effects of the installation position of a multi-radial swirling air-curtain generator on dust diffusion and pollution rules in a fully-mechanized excavation face: A case study”, *Powder Technol.*, **329**, 371-385.
- Lu, C.P., Liu, G.J., Liu, Y., Zhang, N., Xue, J.H. and Zhang, L. (2015), “Microseismic multi-parameter characteristics of rockburst hazard induced by hard roof fall and high stress concentration”, *Int. J. Rock Mech. Min. Sci.*, **76**, 18-32.
- Pan, Y.S., Li, Z.H. and Zhang, M.T. (2003), “Distribution, type, mechanism and prevention of rockburst in China”, *Chin. J. Rock Mech. Eng.*, **22**(11), 1844-1851 (in Chinese).
- Park, J.W. and Song, J.J. (2009), “Numerical simulation of a direct shear test on a rock joint using a bonded-particle model”, *Int. J. Rock Mech. Min. Sci.*, **46**(8), 1315-1328.
- Petukhov, I.M. and Linkov, A.M. (1979), “The theory of post-failure deformations and the problem of stability in rock mechanics” *Int. J. Rock Mech. Min. Sci.*, **16**(2), 57-76.
- Wang, F., Jiang, B.Y., Chen, S.J. and Ren, M.Z. (2019), “Surface collapse control under thick unconsolidated layers by backfilling strip mining in coal mines”, *Int. J. Rock Mech. Min. Sci.*, **113**, 268-277.
- Wang, H., Nie, W., Cheng, W.M., Liu, Q. and Hu, J. (2017), “Effects of air volume ratio parameters on air curtain dust suppression in a rock tunnel’s fully-mechanized working face”, *Adv. Powder Technol.*, **29**(2), 230-244.
- Xie, G.X., Chang, J.C. and Hua, X.Z. (2007), “Influence of mining velocity on mechanical characteristics of surrounding rock in fully mechanized top-coal caving face”, *Chin. J. Geotech. Eng.*, **29**(7), 963-967 (in Chinese).
- Xing, R.J., Meng, X.R. and Wang, P. (2017), “Influence of isolated coal pillar pressure-relieving mining on surrounding rock stability of underlying main roadway”, *Coal Eng.*, **49**(S1), 82-85 (in Chinese).
- Yang, S.L., Wang, Z.H., Jiang, W. and Yang, J.H. (2016), “Advancing rate effect on rock and coal failure format in high-intensity mining face”, *J. China Coal Soc.*, **41**(3), 586-594 (in Chinese).
- Yin, D.W., Chen, S.J., Chen, B., Liu, X.Q. and Ma, H.F. (2018a), “Strength and failure characteristics of the rock-coal combined body with single joint in coal”, *Geomech. Eng.*, **15**(5), 1113-1124.
- Yin, D.W., Chen, S.J., Liu, X.Q. and Ma, H.F. (2018b), “Effect of joint angle in coal on failure mechanical behavior of rock-coal combined body”, *Q. J. Eng. Geol. Hydrogeol.*, **51**(2), 202-209.
- Yin, X.T., Ge, X.R., Li, C.G. and Wang, S.L. (2010). “Influences of loading rates on mechanical behaviors of rock materials”, *Chin. J. Rock Mech. Eng.*, **29**(S1), 2610-2615 (in Chinese).
- Zhang, H.W., Li, Y.P., Chen, Y., Zhu, F. and Shao, L.F. (2017), “Study on safety pushing forward speed of island coal mining face under hard roof and hard seam and hard floor conditions”, *Coal Sci. Technol.*, **45**(5), 6-11(in Chinese).
- Zhang, X.P., Jiang, Y.J., Wang, G., Wang, J.C., Wu, X.Z. and Zhang, Y.Z. (2016), “Numerical experimental on rate-dependent behaviors of granite based on particle discrete element model”, *Rock Soil Mech.*, **37**(9), 2679-2686 (in Chinese).
- Zhao, T.B., Guo, W.Y., Lu, C.P. and Zhao, G.M. (2016), “Failure characteristics of combined coal-rock with different interfacial angles”, *Geomech. Eng.*, **11**(3), 345-359.
- Zhao, W.H., Huang, R.Q. and Yan, M. (2015), “Mechanical and fracture behavior of rock mass with parallel concentrated joints with different dip angle and number based on PFC simulation”, *Geomech. Eng.*, **8**(6), 757-767.
- Zhao, Z.H., Wang, W.M., Dai, C.Q. and Yan, J.X. (2014), “Failure characteristics of three-body model composed of rock and coal with different strength and stiffness”, *T. Nonferr. Metal. Soc. China*, **24**(5), 1538-1546.
- Zuo, J.P., Xie, H.P., Meng, B.B. and Liu, J.F. (2011), “Experimental research on loading-unloading behavior of coal-rock combination bodies at different stress levels”, *Rock Soil Mech.*, **32**(5), 1287-1296 (in Chinese).